2008 IEEE International Conference on
Robotics and Automation
Pasadena, CA, USA, May 19-23, 2008

Skilled-Motion Plannings of Multi-Body Systems Based upon Riemannian Distance

Masahiro Sekimoto, Suguru Arimoto, Sadao Kawamura, and Ji-Hun Bae

Abstract— **This paper focuses on the Riemannian distance and its application to skilled-motion plannings for the system. The Riemannian distance from one pose to another and vice versa is defined as the minimum curve-length measured by the Riemannian metric based upon the system inertia matrix among all curves connecting the two poses. The minimum-length curve in this meaning is called "geodesic" and reflects a movement of the system affected only by inertia-tensor-originated force (*i.e.*, pure inertia, centrifugal, and Coriolis forces). In order to investigate in detail such a movement along the geodesic, some computer simulations are conducted in the cases of planar motions by a 4-DOF robot arm and biped walkings by a whole-body robot. It is shown through simulation results that movements attaining the Riemannian distance (natural movements in inertial actions) in the two cases tend to be similar to those in human skilled motions when human-scale robot models are chosen. Based upon the Riemannian distance, motion plannings for multi-body systems using physical properties inherent in their own physical structures are discussed.**

I. INTRODUCTION

Work space of robots is steadily closer to that of humans and, instead of large-scale industrial robots with hard joints, soft (high back-drivability) robots as assistant robots or humanoid robots have been developed [1], [2]. When such low gear-ratio robots act at the same speeds as humans do, influence of robot-link inertias becomes dominant. In robot control, the inertia term is often treated as a troublesome source rendering strong nonlinearities and couplings among joints. Thus, it has been recommended traditionally in the research of both robot motion planning and control that such troublesome terms should be compensated by a computed torque method. However, we know that inertial actions are used efficiently when we drive a car. Such inertial effect on a "particle" is known as Newton's first law of motion, and inertial actions are used in various situations of everyday life. Therefore, understanding and using inertia-originated effects inherent in multi-body systems must lead to the enhancement of dexterity of robot motions.

Most motion plannings for multi-joint robots have been considered on the basis of optimization of a cost function. The optimal trajectory is numerically derived by introducing a cost function such as maximization of manipulability [3], minimization of quadratic criterion [4], kinetic energy [5], or joint torque [6], obstacle avoidance [7], or avoidance of joint limits [8]. On the other hand, in physiology (particularly, neuro-physiology), some cost functions have been suggested in order to analyze generations of human multi-joint movements. Morasso [9] has reported typical characteristics observed in human skilled reaching: Endpoint position trajectories become quasi-straight and velocity profiles are bell-shaped. As a motion planning model which exhibits such typical characteristics in human reaching, a cost function such as a quadratic criterion of jerk [10] or torque-change [11] has been proposed. However, the issue how inertial movements of a multi-body system should be formulated has not yet been fully discussed.

This paper extends the concept of length of an inertial movement from one point to another of a particle governed by Newton's first law to that of a multi-body system by introducing the Riemannian distance. That is, it deals with an inertia-originated movement from one pose to another of a multi-body system based upon the Riemannian distance. In order to gain a physical insight into multi-joint movements with this distance, some computer simulations are conducted in the cases of planar motions by a 4-DOF (degree of freedom) robot arm and biped walkings by a whole-body robot. These simulation results exhibit a feature that movements attaining the Riemannian distance vary sensitively according to alteration of mass balance among links. Nevertheless, if the physical parameters of these robots are coincident with those of human, quasi-straight endpoint trajectories are observed in multi-joint reachings by the 4-DOF planar robot arm. Similarly, in the case of bipedal walking, knee flexion is admitted. Taking advantage of these noteworthy features, skilled-motion plannings for multi-joint robots using the inertia-originated effects are proposed. The method is free from redundancy of joint DOFs in comparison of the dimension of the endpoint task space. Simulation results show that unexpected behaviors in multi-joint movements such as self-motion can be prevented naturally in the proposed plannings.

II. MOVEMENTS OF MULTI-BODY SYSTEMS BY INERTIAL ACTIONS

As shown in Fig.1, first consider that a particle with mass m moves on a horizontal plane without being affected by gravity or friction between the particle and the plane. Then, it moves from a position $\boldsymbol{x}_s = (x_s, y_s)^{\mathrm{T}}$ to another $\boldsymbol{x}_f = (x_f, y_f)^{\mathrm{T}}$ without decrease or increase of the kinetic energy (that is, no external force acts on the particle). Such

This work was partially supported by the Grant-in-Aid for MEXT. HAITEKU (2004–2008).

M. Sekimoto, S. Arimoto, and S. Kawamura are with the Department of Robotics, Ritsumeikan University, 1-1-1 Nojihigashi, Kusatsu, Shiga 525-8577, Japan sekimoto@fc.ritsumei.ac.jp, {arimoto, kawamura}@se.ritsumei.ac.jp

J.-H. Bae is with the Pohang Institute of Intelligent Robotics, San 31, Hyoja-Dong Nam-Gu, Pohang, Gyeongbuk 790-784, Korea joseph@postech.ac.kr

S. Arimoto is also with the BMC Research Center, RIKEN, 2271-130 Anagahora, Shimoshidami, Moriyama, Nagoya, Aichi 463-0003, Japan

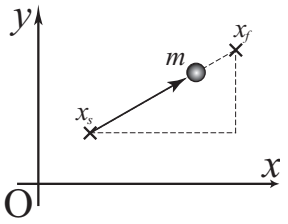

Fig. 1. A movement of a particle

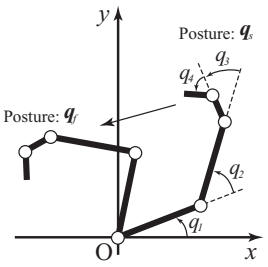

Fig. 2. Planar movements by a robot arm with four DOFs.

a movement is known as "the law of inertia (Newton's first law)" and the particle moves straight between the two points.

This result can be confirmed by solving a two-point boundary value problem. Newton's equation of motion of the particle is described by

$$m\frac{\mathrm{d}^2\boldsymbol{x}}{\mathrm{d}t^2} = \boldsymbol{F} \tag{1}$$

where m denotes the mass, $\boldsymbol{x} \in \Re^2$ the location expressed in terms of the Cartesian coordinates $(O-xy)$, and $\boldsymbol{F} \in \Re^2$ the force acting on the particle. If there is no external force ($\boldsymbol{F} = \boldsymbol{0}$), then the velocity vector $\dot{\boldsymbol{x}}(= \mathrm{d}\boldsymbol{x}/\mathrm{d}t)$ becomes constant and hence the movement of the particle constitutes a straight line from $\boldsymbol{x}_s$ to $\boldsymbol{x}_f$. Along its movement on the line, the kinetic energy is conserved. Conversely, consider any smooth curve $\boldsymbol{x}(t)$ expressed in terms of time variable $t \in [0,1]$ connecting the two points $\boldsymbol{x}(0) = \boldsymbol{x}_s$ and $\boldsymbol{x}(1) = \boldsymbol{x}_f$ and define the quantity

$$d(\boldsymbol{x}_s, \boldsymbol{x}_f) = \min\int_0^1 \sqrt{\frac{1}{2}m\dot{\boldsymbol{x}}(t)^{\mathrm{T}}\dot{\boldsymbol{x}}(t)}\ \mathrm{d}t \tag{2}$$

where minimization is taken over the set of all such smooth curves. Then, it is known that minimization of the right-hand side of eq.(2) is equivalent to solving the differential equation

$$m\frac{\mathrm{d}^2\boldsymbol{x}}{\mathrm{d}t^2} = \boldsymbol{0} \tag{3}$$

with the boundary conditions $\boldsymbol{x}(0) = \boldsymbol{x}_s$ and $\boldsymbol{x}(1) = \boldsymbol{x}_f$. Therefore the movement when the kinetic energy is conserved can be derived by solving this two-point boundary value problem.

In this paper, we focus on inertial movements of a robot arm with multi-joints as shown in Fig.2. Lagrange's equation of motion of the multi-joint arm whose motion is confined to a horizontal plane [12] is described by:

$$\boldsymbol{H}(\boldsymbol{q})\ddot{\boldsymbol{q}} + \left\{\frac{1}{2}\dot{\boldsymbol{H}}(\boldsymbol{q}) + \boldsymbol{S}(\boldsymbol{q},\dot{\boldsymbol{q}})\right\}\dot{\boldsymbol{q}} = \boldsymbol{u} \tag{4}$$

where $\boldsymbol{q} \in \Re^n$ denotes the vector of joint angles, $\boldsymbol{H}(\boldsymbol{q}) \in \Re^{n\times n}$ the inertia matrix, $\boldsymbol{S}(\boldsymbol{q},\dot{\boldsymbol{q}}) \in \Re^{n\times n}$ a skew-symmetric matrix, and $\boldsymbol{S}(\boldsymbol{q},\dot{\boldsymbol{q}})\dot{\boldsymbol{q}}$ the gyroscopic force term including centrifugal and Coriolis forces, $\boldsymbol{u} \in \Re^n$ the control input torque at joints. The integer n corresponds to the number of DOFs of the system. The set of all joint vectors $(q_1, \ldots, q_n)$ is called "configuration space." A point on a configuration space can be corresponded to a pose of the robot.

We now consider a movement when the multi-joint robot moves from a pose $\boldsymbol{q}_s$ to another $\boldsymbol{q}_f$. Such a movement can be described as $\boldsymbol{q}(t)$ by using the parameter $t \in [0,1]$, where $\boldsymbol{q}(0) = \boldsymbol{q}_s$ and $\boldsymbol{q}(1) = \boldsymbol{q}_f$, and then, the inertia matrix of robot $\boldsymbol{H}(\boldsymbol{q}(t)) = (h_{ij}(\boldsymbol{q}(t)))$ is certainly determined corresponding to each pose. An inertial movement of a multi-joint arm can be derived in a way similar to the case of a particle by solving the minimization problem of the following quantity:

$$R(\boldsymbol{q}_s, \boldsymbol{q}_f) = \min\int_0^1 \sqrt{\frac{1}{2}\sum_{i,j=1}^{n} h_{ij}(\boldsymbol{q}(t))\dot{q}_i(t)\dot{q}_j(t)}\ \mathrm{d}t \tag{5}$$

where minimization is taken over all smooth trajectories $\boldsymbol{q}(t)$ with satisfying the boundary conditions $\boldsymbol{q}(0) = \boldsymbol{q}_s$ and $\boldsymbol{q}(1) = \boldsymbol{q}_f$. The quantity is called "Riemannian distance" and the solution trajectory $\boldsymbol{q}(t)$ minimizing the integral in eq.(5) is called "geodesic." This trajectory is obtained by solving the two-point boundary value problem regarding the differential equation

$$\boldsymbol{H}(\boldsymbol{q})\ddot{\boldsymbol{q}} + \left\{\frac{1}{2}\dot{\boldsymbol{H}}(\boldsymbol{q}) + \boldsymbol{S}(\boldsymbol{q},\dot{\boldsymbol{q}})\right\}\dot{\boldsymbol{q}} = \boldsymbol{0} \tag{6}$$

with the boundary conditions $\boldsymbol{q}(0) = \boldsymbol{q}_s$ and $\boldsymbol{q}(1) = \boldsymbol{q}_f$. In this paper, we also focus on the Riemannian distance $R(\boldsymbol{q}_s, \boldsymbol{q}_f)$ together with the movement corresponding to the geodesic that must conserve the kinetic energy. This distance possesses the following properties.

(1) The Riemannian distance is independent of choice of the time parameter t.
(2) On the trajectory $\boldsymbol{q}(t)$ (geodesic) realizing the Riemannian distance, the kinetic energy is constant.

Even if the parameter t is replaced by any monotonically increasing function $s(t)$ in $[s(0), s(1)]$, the Riemannian distance is invariant. The second statement is obvious because taking an inner product between eq.(6) and $\dot{\boldsymbol{q}}$ yields

$$\frac{\mathrm{d}}{\mathrm{d}t}\left(\frac{1}{2}\dot{\boldsymbol{q}}^{\mathrm{T}}\boldsymbol{H}(\boldsymbol{q})\dot{\boldsymbol{q}}\right) = \frac{\mathrm{d}}{\mathrm{d}t}K = 0 \tag{7}$$

In differential geometry [13]–[15], eq.(6) is called the Euler-Lagrange equation and expressed by

$$\sum_{j=1}^{n} h_{ij}(\boldsymbol{q})\,\ddot{q}_j + \sum_{j=1}^{n}\sum_{k=1}^{n}\Gamma_{ijk}(\boldsymbol{q})\,\dot{q}_j\dot{q}_k = 0 \qquad (i = 1, \ldots, n) \tag{8}$$

where $h_{ij}(\boldsymbol{q})$ denotes the ij-entry of inertia matrix $H(\boldsymbol{q})$ and $\Gamma_{ijk}(\boldsymbol{q})$ expresses Christoffel's symbol. The set of all possible poses of the robot constitutes a smooth manifold expressed by the symbol $(\mathcal{M}, p)$, where p represents a pose and can be corresponded to local coordinates $(q_1, \ldots, q_n)$. If the smooth manifold $(\mathcal{M}, p)$ is connected and associated with the Riemannian distance defined above, it is called the Riemannian manifold and denoted by $(\mathcal{M}, p, h_{ij}(p))$.

TABLE I

PHYSICAL PARAMETERS OF THE ARMS

Link number	i	1	2	3	4
Length [m]	l_i	0.2800	0.2800	0.09500	0.09000
Center of mass [m]	l_{gi}	0.1400	0.1400	0.04750	0.04500
Cylinder radius [m]	r_i	0.04000	0.03500	N/A	0.009500
Cuboid height [m]	h_i	N/A	N/A	0.08500	N/A
Cuboid depth [m]	d_i	N/A	N/A	0.03000	N/A
Mass [kg]	m_i	1.407	1.078	0.2423	0.02552
Inertia moment [kgm^2]	I_{giz}	9.758×10^{-3}	7.370×10^{-3}	2.004×10^{-4}	1.780×10^{-5}

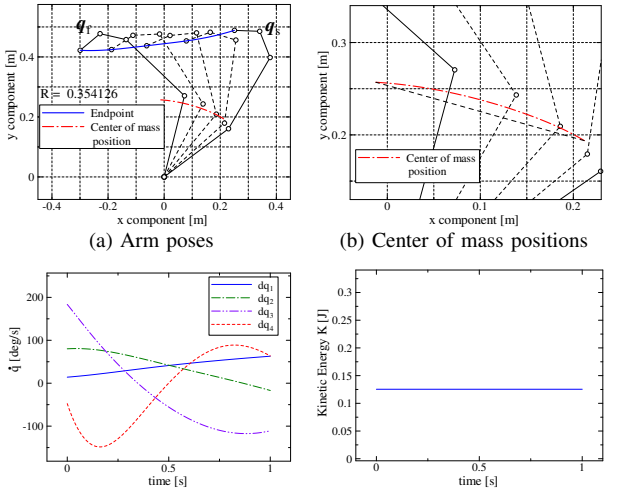

(a) Arm poses (b) Center of mass positions

(c) Joint angular velocities $\dot{\boldsymbol{q}}$ (d) Kinetic energy K

Fig. 3. Transient responses of the whole arm in the movement attaining the Riemannian Distance

III. NUMERICAL SIMULATIONS

By using the 4-DOF robot arm shown in Fig.2, some numerical simulations are carried out in order to investigate movements attaining the Riemannian distance (*i.e.*, multi-joint movements by inertial actions). Physical parameters of the robot are determined as in TABLE I corresponding to the size of human adult upper limb.

Figure 3 shows the trajectory of geodesic $\boldsymbol{q}(t)$ when the two-point boundary value problem is solved under the differential equation of eq.(6) and the boundary conditions $\boldsymbol{q}(0) = \boldsymbol{q}_s$ and $\boldsymbol{q}(T) = \boldsymbol{q}_f$, where $T = 1$[s] and

$$\begin{cases} \boldsymbol{q}_s = (35.0,\ 23.0,\ 55.0,\ 65.0)^{\mathrm{T}}\ [\mathrm{deg}] \\ \boldsymbol{q}_f = (75.0,\ 63.0,\ 30.0,\ 50.0)^{\mathrm{T}}\ [\mathrm{deg}] \end{cases} \tag{9}$$

Figure 3(a) shows the pose transition corresponding to the geodesic $\boldsymbol{q}(t)$. Unlike an intuition that the trajectory of the center of mass (COM) of the multi-joint arm may become straight in task space (Cartesian space) because a particle moves straight in inertial movements, the trajectory of COM does not become straight as shown in Fig.3(b). Further, differently from movements of a particle, the angular velocities of the geodesic are not constant as shown in Fig.3(c) whereas the kinetic energy K is constant during movements as shown in Fig.3(d).

Figure 4 shows the endpoint trajectories in task space corresponding to each geodesic when mass balance of the robot is altered. Figure 4(a) shows simulation results when the value of mass of the second link m_2 is changed, and Fig.4(b) shows results when that of the end link m_4 is changed. As shown in both simulation results, alteration of

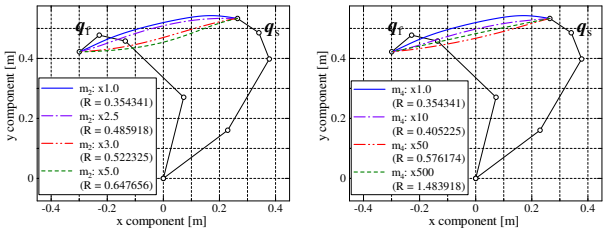

(a) m_2 is changed (b) m_4 is changed

Fig. 4. Transient responses of movements given by the geodesics when the mass balances of the arm are altered

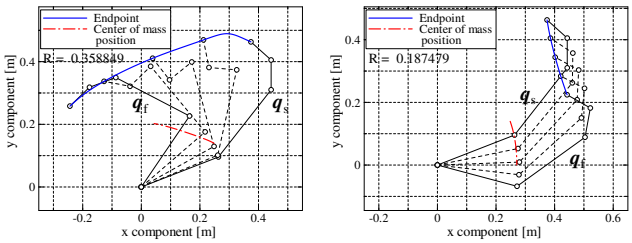

(a) $\boldsymbol{q}_f = (54,\ 100,\ 45,\ 23)^{\mathrm{T}}$[deg] (b) $\boldsymbol{q}_f = (-14,\ 48,\ 45,\ 73)^{\mathrm{T}}$[deg]

Fig. 5. Transient responses of movements given by the geodesics when $\boldsymbol{q}_s = (20.0,\ 30.0,\ 40.0,\ 50.0)^{\mathrm{T}}$ [deg] is given and $\boldsymbol{q}_f$ is changed.

the mass balance directly affects the geodesic. Further, each Riemannian distance differs according to alteration of the mass balance though both boundary conditions are fixed. It suggests that the Riemannian distance reflects physical properties (inertia-induced effects) of multi-joint movements and appropriately exhibits the distance between two poses in a dynamic sense.

Figure 5 shows the endpoint trajectories and the pose transition in task space corresponding to the geodesic when $\boldsymbol{q}_s$ is fixed but $\boldsymbol{q}_f$ is changed. In these simulations, an interesting phenomenon is observed that the endpoint trajectories tend to be straight when the human-scaled parameters are set in the robot model despite that only inertia-originated movements are taken into account (see Fig.5(b)). This result may become interesting if we refer to the well-known result in neuro-motor physiology that the endpoint trajectory of human skilled point-to-point reaching becomes quasi-straight [9]. It also suggests that the balance of mass distribution of human upper-limb plays one of key roles in acquirements of motor skill and dexterity.

IV. HUMAN WALKING

In order to gain a physical insight into inertia-originated movements given by the Riemannian distance, we focus on a swing phase of human walking (Fig.6) as another example. Humans bend their knee during the swing phase of walking to prevent from stubbing their toes against the ground. However, they usually walk almost without intention though its motion is the most dynamic in human walking. This suggests that such knee flexion in dynamic walking is generated dominantly by inertia-originated actions. By observing the multi-joint movements based upon the Riemannian distance in computer simulations, such a behavior in biped walking is confirmed.

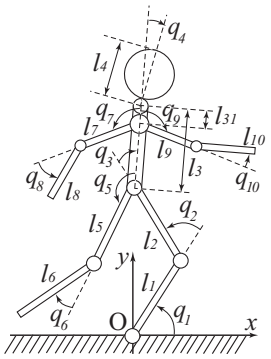

Fig. 6. A human-like whole body model

TABLE II

PHYSICAL PARAMETERS OF THE WALKING MODEL

Link number (i)	Length [m] (l_i)	Center of mass [m] (l_{gi})	Mass [kg] (m_i)	Inertia moment [kgm^2] (I_{giz})
Lower thigh (1, 6)	0.45	0.27	4.68	8.285×10^{-2}
Thigh (2, 5)	0.40	0.24	6.50	9.507×10^{-2}
Torso (3)	0.60	0.30	33.28	1.145×10^{0}
Head (4)	0.20	0.08	2.86	1.279×10^{-2}
Upper arm (7, 9)	0.28	0.14	1.625	1.137×10^{-2}
Forearm (8, 10)	0.28	0.14	1.625	1.137×10^{-2}

Differently from planar movements by the 4-DOF robot arm, the whole-body model consists of branched links. Nevertheless, when its motions are constrained on the sagittal plane (xy-plane), Lagrange's equation of motion of the model is described in the same formula as eq.(4). As described above, the size effect becomes considerably important in an inertia-originated movement attaining the Riemannian distance. Thus, the size corresponding to that of human with respect to length and mass (height: 1.65[m], weight: 65[kg]) was set as in TABLE II, and numerical simulations were conducted.

Figure 7 shows simulation results when the two-point boundary value problem was solved under the differential equation of eq.(6) and the boundary conditions determined by the two poses ($\boldsymbol{q}_s$ and $\boldsymbol{q}_f$) as illustrated in Fig.7. In Fig.7, we show the pose transition from $\boldsymbol{q}_s$ to $\boldsymbol{q}_f$ in task space given by the geodesic in solid lines and, to make the features of the geodesic in this case elucidative, we also show the transition of another movement when each joint angular velocity is taken to be constant during the movement from $\boldsymbol{q}_s$ to $\boldsymbol{q}_f$ in broken lines. The movement attaining the Riemannian distance slightly exhibits knee flexion in comparison with that in constant angular velocities. In order to investigate in detail such an effect, another simulation was conducted as shown in Fig.8. Figure 8 demonstrates the noticeable knee flexion. From these results, it is possible to claim that a principal factor of the skilled body-movement during the swing phase of walking by the human-scaled model must be governed by the inertia-originated action without using any intentional control.

V. HUMAN REACHING

Motion generations for human reaching movements under the circumstances of joint redundancy were discussed from the viewpoint of Newtonian mechanics in the literature [16]–[18]. In particular, in the paper [16] it is assumed that a set of joint torques generates a force at the endpoint as if the endpoint were pulled by a virtual spring whose potential takes its minimum at the target point of reaching. When a set of dampings at joints together with a stiffness of virtual spring are coordinately adjusted, the generated motions considerably resemble motions observed typically in human skilled reaching (*i.e.*, straight endpoint position trajectories and bell-shaped endpoint velocity profiles). The control signal for generating such a motion is given as follows:

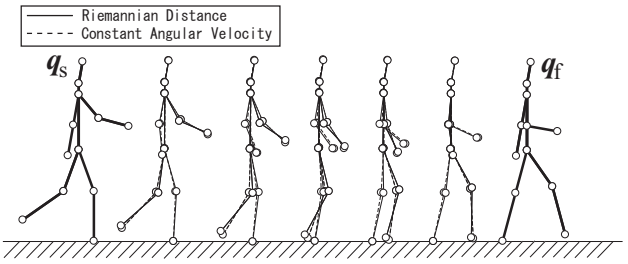

Fig. 7. Posture transition in biped walking based upon the Riemannian distance

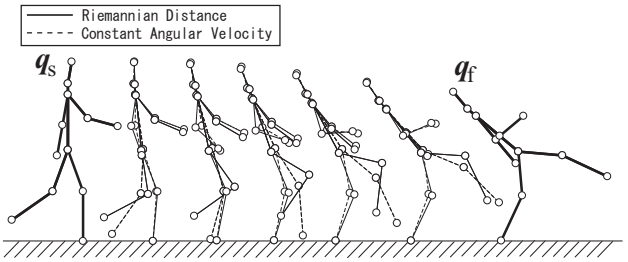

Fig. 8. Posture transition in kick motion based upon the Riemannian distance

$$\begin{cases} \boldsymbol{u} = -\boldsymbol{C}\dot{\boldsymbol{q}} - \boldsymbol{J}^{\mathrm{T}}(\boldsymbol{q})\left\{k\Delta\boldsymbol{x} + \zeta_1\sqrt{k}\dot{\boldsymbol{x}}\right\} \\ \boldsymbol{C} = \mathrm{diag}(c_1, c_2, c_3, c_4) \\ c_i = \zeta_0\sqrt{k}\sqrt{\displaystyle\sum_{j=1}^{4}|h_{ij}(\boldsymbol{q}(0))|} \end{cases} \tag{10}$$

and this idea has been called "Virtual spring-damper (VSD) hypothesis [17]." In eq.(10), $\boldsymbol{C} \in \Re^{4\times4}$ denotes the positive definite and diagonal damping coefficient matrix, $\boldsymbol{J}(\boldsymbol{q}) \in \Re^{2\times4}$ the Jacobian matrix of task coordinates $\boldsymbol{x}$ in joint coordinates $\boldsymbol{q}$, $\Delta\boldsymbol{x}(t) = \boldsymbol{x}(t) - \boldsymbol{x}_d(t)$, $\boldsymbol{x}$ the endpoint position, $\boldsymbol{x}_d$ the target position, and k, ζ_0, and ζ_1 are the positive constant gain parameters.

In order to evaluate this movement with the Riemannian distance, numerical simulations were conducted under the same condition in the three cases: a movement generated by the VSD hypothesis, that attaining the Riemannian distance of eq.(5), and that generated by a generally-known PD feedback method in joint space. Simulations were conducted in the case of the four-DOF planar robot arm depicted in Fig.2 whose parameters were set as in TABLE I. Firstly, by using the control signal in eq.(10), a computer simulation was conducted when the initial posture, target point, and gain parameters were set as shown in TABLE III. The endpoint eventually converged to the target point and the robot was

TABLE III

INITIAL VALUES AND GAIN SETTINGS FOR THE VSD

Initial posture	$q_1(0)$	39.0 [deg]
	$q_2(0)$	63.0 [deg]
	$q_3(0)$	25.0 [deg]
	$q_4(0)$	85.0 [deg]
Initial endpoint	$x(0)$	0.02589 [m]
	$y(0)$	0.4783 [m]

Gains	k	20 [N/m]
	ζ_0	0.2 [-]
	ζ_1	1.7 [-]
Desired position	x_d	-0.2 [m]
	y_d	0.4 [m]

TABLE IV

THE FINAL POSTURE IN THE MOVEMENT OF THE VSD

Convergence time	T	2.5 [s]
Initial posture	$q_1(T)$	55.52 [deg]
	$q_2(T)$	78.59 [deg]
	$q_3(T)$	31.92 [deg]
	$q_4(T)$	51.46 [deg]
Initial endpoint	$x(T)$	-0.2 [m]
	$y(T)$	0.4 [m]

in still state at $T = 2.5$[s]. The final pose of the robot in still state is shown in TABLE IV. Next, by setting the initial pose $\boldsymbol{q}(0)$ and the final pose $\boldsymbol{q}(T)$ in TABLEs III and IV as the boundary conditions, the geodesic $\boldsymbol{q}(t)$ was derived from eq.(6). Finally, a computer simulation was conducted by using the control signal

$$\boldsymbol{u} = -\boldsymbol{k}_{dq}\dot{\boldsymbol{q}}(t) - \boldsymbol{k}_{pq}(\boldsymbol{q}(t) - \boldsymbol{q}_d) \tag{11}$$

where $\boldsymbol{k}_{dq}$ and $\boldsymbol{k}_{dp}$ denote diagonal matrices respectively. The initial pose in TABLE III was set and the final pose in TABLE IV was set as the desired angle $\boldsymbol{q}_d$. The gain parameters $\boldsymbol{k}_{dq}$ and $\boldsymbol{k}_{dp}$ were, so as to finish the task at $T = 2.5$[s], determined as follows:

$$\begin{cases} \boldsymbol{k}_{dq} = \mathrm{diag}(1.29, 0.85, 0.60, 0.50)\ [\mathrm{Nms/rad}] \\ \boldsymbol{k}_{pq} = \mathrm{diag}(1.8, 1.5, 1.5, 1.5)\ [\mathrm{Nm/rad}] \end{cases} \tag{12}$$

Figure 9 shows the simulation results, where PD denotes a movement by the PD feedback control at joint level, VSD that by the control signal based upon the VSD hypothesis, and RD that by the geodesic. As seen in Figs.9(a) and 9(b), the endpoint trajectory of the VSD is significantly close to that of the RD. However, as shown in Fig.9(c), transient responses of the joint angle q_3 are considerably different. In order to compare movements actually generated by using a special controller $\boldsymbol{u}$ with the geodesic, we introduce the quantity defined by

$$R_u = \int_0^\infty \sqrt{\frac{1}{2}\sum_{i,j} h_{ij}(\boldsymbol{q}(t))\,\dot{q}_i(t)\dot{q}_j(t)}\ \mathrm{d}t \tag{13}$$

corresponding to the Riemannian distance. The quantities R_u measured along movements of the VSD and the PD are finite because the proof of stability and exponential convergence concerning these movements has been given [12], [16]. Further, these quantities are surely larger than the Riemannian distance $R(\boldsymbol{q}_s, \boldsymbol{q}_f)$. If the quantity is closer to the Riemannian distance, it is considered that its movement is close to an inertia-originated movement. In Fig.9, the quantities in the two cases (the VSD and the PD) are close to the Riemannian distance. However, the quantity of the VSD is much larger than that of the PD though the endpoint trajectory of the VSD is considerably close to that of the RD.

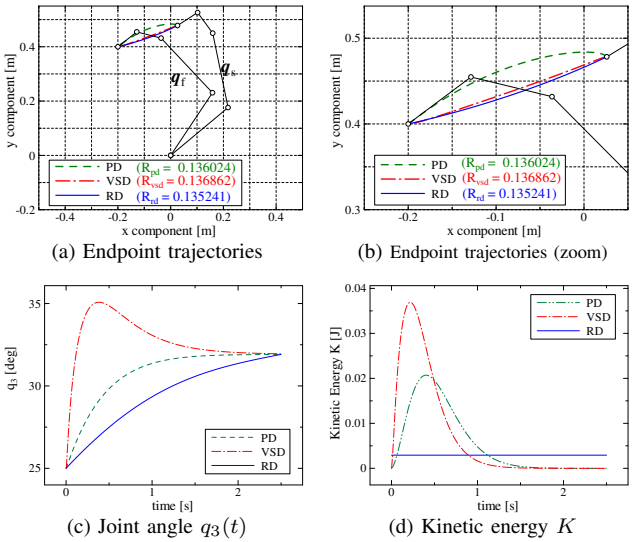

(a) Endpoint trajectories (b) Endpoint trajectories (zoom)

(c) Joint angle $q_3(t)$ (d) Kinetic energy K

Fig. 9. Comparisons of movements by two controllers (PD and VSD) with the movement attaining the Riemannian distance in the case of middle-range reaching

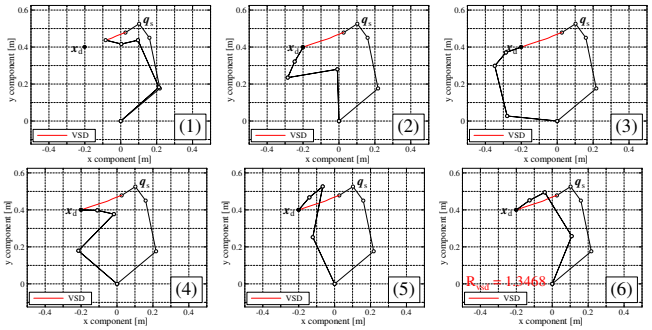

Fig. 10. An unexpected self-motion

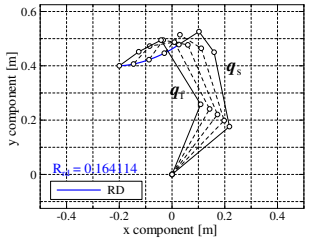

Fig. 11. A trajectory in task space given by the geodesic when an unexpected self-motion is incurred

Further, Fig.9(d) shows that the kinetic energy of the VSD is large in comparison with the others and surplus energy is consumed.

Figure 10 shows the simulation results when the gain parameters in the control signal based upon the VSD hypothesis of eq.(10) are inappropriately determined. In this case, the robot starts to move and its endpoint reaches the target point. However, each joint continues to move for a certain period while keeping the endpoint at the target. After a while, the robot recovers from over-shootings and finally becomes in still state at the pose of $\boldsymbol{q}_f$. From this result, it is possible to set the initial and final poses as the boundary conditions and to derive the geodesic curve. Figure 11 shows the pose transition given by the geodesic in this case. The phenomenon in Fig.10 is called "self-

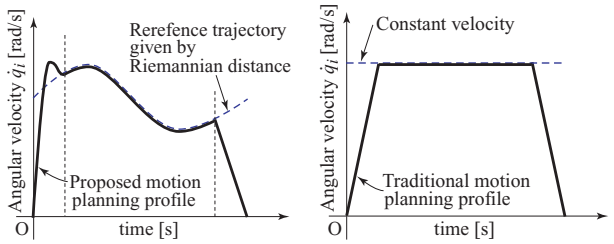

(a) Proposed planning (b) Traditional planning

Fig. 12. A motion planning based upon the Riemannian distance

motion [19]" and it sometimes incurs unexpected behavior. However, Fig.11 shows that the movement given by the Riemannian distance does not incur such an unexpected self-motion. On the other hand, the quantity of eq.(13) in Fig.10 becomes extremely larger than the Riemannian distance in Fig.11. It suggests that such an unexpected self-motion can be distinguished by using this distance.

VI. MOTION PLANNINGS BASED UPON THE RIEMANNIAN DISTANCE

In order to generate more dexterous PTP movements from one pose to another of multi-joint robots, motion plannings using the Riemannian distance are proposed. Movements given by the Riemannian distance cannot be directly applied to PTP motion plannings because the still states (zero velocities) at the initial and final poses are not supposed. However, the strategy as shown in Fig.12(a) is effective: Actuator torques are instantly exerted over the system so as to make the system ride on inertia-induced movements as soon as possible at the starting stage. After that the system moves in its movement without exerting forces, and finally in the vicinity of the target the kinetic energy in the system should be quickly dissipated. This resembles the traditional PTP control for industrial robots using a trapezoidally-shaped velocity profile as shown in Fig.12(b). However, differently from this conventional method, the proposed motion plannings are designed so as to keep the kinetic energy constant. Taking advantage of the Riemannian distance, the method generates skilled motions without compensating the strong non-linearities and coupling effects in multi-joint movement. This method is particularly suitable for controlling robots with low gear-ratio, low frictions, and strong non-linearities at joints.

We discuss more in detail how to maneuver the system on the inertial movement at a starting stage and to the specified pose at a final stage. First, the reference trajectories given by the Riemannian distance $(\boldsymbol{q}_r(t), \dot{\boldsymbol{q}}_r(t))$ can be derived by solving eq.(6) under the boundary conditions given by the initial and target poses. Then, the robot is permitted to track on such trajectories only if at time t during its movement the system state $(\boldsymbol{q}(t), \dot{\boldsymbol{q}}(t))$ is coincident with that given by the geodesic $(\boldsymbol{q}_r(t), \dot{\boldsymbol{q}}_r(t))$. Here, two approaches to achieve it are suggested: One is an on-line approach in which the system is exerted feedforwardly impulsive forces through its joints so as to attain the geodesic instantly at the starting stage and then it converges to the target pose by using a sliding mode control at a final stage. Another is an off-line approach in which the system is controlled along the motion profile designed in advance as shown in Fig.12(a).

VII. CONCLUSIONS

Inertia-originated movements of a multi-body system based upon the Riemannian distance and its use in skilled-motion plannings were discussed. In future works, the effectiveness of the proposed motion plannings will be verified.

REFERENCES

[1] (2007) The KUKA Roboter GmbH website. [Online]. Available: http://www.kuka.com/en/

[2] G. Cheng, S.-H. Hyon, J. Morimoto, A. Ude, J. G. Hale, G. Colvin, W. Scroggin, and S. C. Jacobsen, "CB: a humanoid research platform for exploring neuroscience," *Advanced Robotics*, vol. 21, no. 10, pp. 1097–1114, 2007.

[3] T. Yoshikawa, "Manipulability of robotic mechanisms," *International Journal of Robotics Research*, vol. 4, no. 2, pp. 3–9, 1985.

[4] D. E. Whitney, "Resolved motion rate control of manipulators and human prostheses," *IEEE Trans. on Man-Machine Systems*, vol. MMS-10, no. 2, pp. 47–53, 1969.

[5] O. Khatib, "A unified approach for motion and force control of robot manipulators: The operational space formulation," *IEEE Journal of Robotics and Automation*, vol. RA-3, no. 1, pp. 43–53, 1987.

[6] J. M. Hollerbach and K. C. Suh, "Redundancy resolution of manipulators through torque optimization," *IEEE Journal of Robotics and Automation*, vol. RA-3, no. 4, pp. 308–316, 1987.

[7] H. Hanafusa, T. Yoshikawa, and Y. Nakamura, "Analysis and control of articulated robot arms with redundancy," in *Proc. of the 8th Triennial World Congress of IFAC*, vol. 4, Kyoto, Japan, 1981, pp. 1927–1932.

[8] A. Liegeois, "Automatic supervisory control of the configuration and behavior of multibody mechanisms," *IEEE Trans. on Systems, Man and Cybernetics*, vol. SMC-7, no. 12, pp. 868–871, 1977.

[9] P. Morasso, "Spatial control of arm movements," *Experimental Brain Research*, vol. 42, no. 2, pp. 223–227, 1981.

[10] T. Flash and N. Hogan, "The coordination of arm movements: an experimentally confirmed mathematical model," *The Journal of Neuroscience*, vol. 5, no. 7, pp. 1688–1703, 1985.

[11] Y. Uno, M. Kawato, and R. Suzuki, "Formation and control of optimal trajectory in human multijoint arm movement. minimum torque-change model," *Biological Cybernetics*, vol. 61, no. 2, pp. 89–101, 1989.

[12] S. Arimoto, *Control Theory of Non-linear Mechanical Systems: A Passivity-based and Circuit-theoretic Approach*. Oxford, UK: Oxford Univ. Press, 1996.

[13] J. Jost, *Riemannian Geometry and Geometric Analysis*. Berlin: Springer, 2002.

[14] V. G. Ivancevic and T. T. Ivancevic, *Geometrical Dynamics of Complex Systems: A Unified Modelling Approach to Physics, Control, Biomechanics, Neurodynamics and Psycho-Socio-Economical Dynamics*. Springer, Berlin, 2006.

[15] F. Bullo and A. D. Lewis, *Geometric Control of Mechanical Systems: Modeling, Analysis, And Design For Simple Mechanical Control Systems*. Springer, New York, 2000.

[16] S. Arimoto, M. Sekimoto, H. Hashiguchi, and R. Ozawa, "Natural resolution of ill-posedness of inverse kinematics for redundant robots: A challenge to Bernstein's degrees-of-freedom problem," *Advanced Robotics*, vol. 19, no. 4, pp. 401–434, 2005.

[17] S. Arimoto, H. Hashiguchi, M. Sekimoto, and R. Ozawa, "Generation of natural motions for redundant multi-joint systems: A differential-geometric approach based upon the principle of least actions," *Journal of Robotic Systems*, vol. 22, no. 11, pp. 583–605, 2005.

[18] S. Arimoto and M. Sekimoto, "Human-like movements of robotic arms with redundant DOFs: Virtual spring-damper hypothesis to tackle the Bernstein problem," in *Proc. of the 2006 IEEE International Conference on Robotics and Automation (ICRA2006)*, Orlando, Florida, USA, May 15-19 2006, pp. 1860–1866.

[19] H. Seraji, "Configuration control of redundant manipulators: theory and implementation," *IEEE Transactions on Robotics and Automation*, vol. 5, no. 4, pp. 472–490, 1989.